Digital acoustic sensor performance across the infrasound range in non-isolated conditions

Karina Asmar, Milton Garcés, Darren Hart, and Brian Williams

Citation: The Journal of the Acoustical Society of America **144**, 3036 (2018); doi: 10.1121/1.5078591
View online: https://doi.org/10.1121/1.5078591
View Table of Contents: https://asa.scitation.org/toc/jas/144/5
Published by the Acoustical Society of America

Digital acoustic sensor performance across the infrasound range in non-isolated conditions

Karina Asmar,[1,a)] Milton Garcés,[1] Darren Hart,[2] and Brian Williams[1]
[1]*Infrasound Laboratory, University of Hawai'i at Manoa, 73970 Makako Bay Drive 205, Kailua-Kona, Hawaii 96740, USA*
[2]*DMH Consulting Services, LLC, 4425 Juan Tabo Boulevard NorthEast, Suite 135, Albuquerque, New Mexico 87111, USA*

(Received 4 June 2018; revised 15 October 2018; accepted 25 October 2018; published online 30 November 2018)

The next generation of acoustic sensors is emerging to supplement legacy sensors traditionally used in regional and global networks. These devices operate under similar principles as traditional sensors, without the need of a separate external digitizer. The calibration of these sensors against their predecessors is crucial to the modernization of conventional technologies. This work describes the characterization of the next-generation MB3 digital microbarometer and the iPrecision smartphone microphone in a non-isolated calibration room across the infrasound (i.e., 0.01–20 Hz) range. The intent is to evaluate nominal instrument performance before deployment. A portable rotary subwoofer is used as a controllable infrasound source to generate single-tone sinusoidal and broadband noise pressure waves in a room configured for calibration purposes. For each device, comparison measurements are made, from which the digital sensitivity and the parametric response is developed. The results provide insight into the performance of the sensors in non-isolated environments. By overlapping the responses of the test sensors, digital sensor performance across the infrasound range can be benchmarked. These responses may serve as a double-reference scheme in future pressure measurements and digital calibrations of acoustic sensors.
 https://doi.org/10.1121/1.5078591

[MJW] Pages: 3036–3045

I. INTRODUCTION

Acoustic sensors use different mechanisms to convert input pressure fluctuations into output analog or digital signals. In order to ensure that the end result of this conversion accurately represents the incoming pressure field, it is necessary to properly characterize and calibrate the sensors performing the measurements (Marcillo *et al.*, 2012). This work describes the evaluation and characterization of two next-generation digital sensors across the infrasound range. These devices are part of a modern generation of acoustic sensors known for the integration of analog-to-digital converters to provide digital data. Their significant reduction in size, weight, power, and cost is also advantageous to data collection and shipping logistics. The calibration of these sensors could potentially contribute to the modernization of conventional acoustic sensing technologies. Though numerous analog acoustic calibrations and chamber tests have been performed and are described in the literature, the calibration methods described in this study focus on the evaluation of the *digital* output of the test sensors relative to established analog reference sensors connected to external digitizers. We define the *digital sensitivity* of an acoustic sensor system (i.e., transducer plus digitizer) as the ratio of the input pressure to the system's digital output. We develop response models for the digital acoustic sensors in terms of *digital gain*, which we define as the ratio of the system's digital output to the input pressure (i.e., the inverse of the digital sensitivity). We use a portable rotary subwoofer (which will be described in Sec. II) as a controllable infrasound source (Park *et al.*, 2009a) in calibration experiments performed in non-isolated conditions.

The first test sensor is the MB3 digital microbarometer (MB3d), an infrasound sensor developed by the Commissariat à l'Énergie Atomique (CEA) to meet the Comprehensive Nuclear-Test-Ban Treaty (CTBT) International Monitoring System (IMS) requirements. This sensor is a newer version of the MB2000 and MB2005 series (Seismowave, 2015). IMS sensors are designed to operate with an enhanced response within the 0.02–4 Hz pass band. A notable feature of the MB3d is the integration of an on-board, low-noise 24-bit analog-to-digital converter (ADC) for digital output. The digitizing block of the MB3d permits time synchronization with universal coordinated time (UTC), which is performed by a time tagging board with pulse per second (PPS) capability. When connected to a global positioning system (GPS) antenna, the digitizing block provides digital data outputs with GPS timestamps, which are known to be accurate to the order of milliseconds. The Hyperion model 5200 series is another example of an existing digital infrasound sensor manufactured for explosion monitoring. Aside from reduced size and weight, the MB3d is reengineered to use a linear variable differential transformer (LVDT) as opposed to a magnet and coil velocity transducer. This last feature is essential for lowering the self-noise of the sensor in the upper passband. The analog version of the MB3d (i.e., the MB3a) was evaluated

[a)]Electronic mail: kasmar@isla.hawaii.edu

by Merchant and McDowell (2014) and Larsonner *et al.* (2014). Although the MB3d and MB3a share the same transducer block and analog response, the digital output of the MB3d is constrained by its embedded digitizer. In this study, we characterize the MB3d digital response against its MB2000 analog predecessor (CEA/DAM, 2009) connected to a conventional 24-bit digitizer Reftek model 130 (Refraction Technology Inc., 2011) commonly used in field experiments.

The second test sensor is the iPrecision smartphone microphone (iMic) (Audio Control, 2018), a factory calibrated iOS condenser microphone with an embedded preamplifier and 24-bit analog-to-digital converter. This device is designed to operate with a flat (within 3 dB) amplitude response from 3 to 20 000 Hz. When connected to an iPhone or an iPad, it is able to bypass the analog electronic stages with a digital audio link and override the internal microphone. In this work, we use the *RedVox Infrasound app* for iOS (Redvox, 2014) to record acoustic signals measured by the iMic. This *app* displays the acoustic pressure recorded with the internal or external microphone as it streams the sound files anonymously to a cloud server for analysis. In this work, we describe the response of the system consisting of the iMic sensor connected to an iPhone 6s. The reference for calibrating the iMic at higher frequencies is the Brüel & Kjaer (B&K) low-frequency pressure-field 1/2 in. microphone type 4193 (Brüel and Kjaer, 1995), which will be described in Sec. IV. B&K microphones are commonly used as references in acoustic calibration processes (Larsonner *et al.*, 2014 and Ollivier *et al.*, 2012) due to their long-established stability and reliability.

This article describes the evaluation and characterization of these next-generation digital sensors against legacy analog sensors configured with external digitizers in a non-isolated calibration room across the 0.01–20 Hz passband. Section II describes the experimental and processing methods applied in the calibration tests and analyses. Section III describes the characterization of the MB3d sensor against its analog MB2000 predecessor across 0.01–4 Hz. We evaluate an analog Brüel & Kjaer Microphone type 4193 against the MB3d in the common passband (0.25–4 Hz) in Sec. IV. This Brüel & Kjaer microphone is then chosen as a reference for calibrating the iMic sensor. Section V subsequently focuses on the calibration of the iMic flat amplitude response against the Brüel & Kjaer sensor across 1–20 Hz. We summarize our observations in Sec. VI and comment on the applications of our results.

II. METHODS

The performance evaluation of the acoustic sensors described in this work took place in a $\sim 10.7 \times 7.3 \times 3.0$ m^3 non-isolated calibration room. External factors such as wind, ambient, and cultural noise were therefore components in the acoustic measurements. All acoustic signals were generated with a Tektronix RM 3100 signal generator. A Thigpen Rotary Woofer model 17 (TRW-17) (Eminent Technologies, 2018 and Park and Robertson, 2009b) was used as the sound projector for frequencies lower than 20 Hz. The TRW-17 is essentially a rotating fan, driven by an electric motor, with blades that pitch dynamically in response to an applied signal. While the fan rotates at constant frequency, an input signal is fed into the system's audio amplifier, which drives a conventional electromagnetic coil assembly. The longitudinal motion of the coil is then converted to rotational motion of the blades (Park *et al.*, 2009a). The result is a sound pressure wave propagating at a frequency determined by the input electrical signal. The TRW-17 described in this study is configured so that it radiates into the calibration room, while a room of dimensions $\sim 8.8 \times 6.6 \times 3.0$ m^3 forms the back volume. Sensors were placed at an approximate distance of 5 meters from the TRW-17 in the calibration room. Three types of tests were performed to assess the response of the sensors. Analog and pressure chamber versions of these tests, described in Secs. II A–II C, are presented in Kromer *et al.* (2007).

Each acoustic sensor's frequency response is defined parametrically as a function of angular frequency ω in terms of amplitude or gain k, poles p_i and zeros z_i (Merchant and Hart, 2011) as

$$H(e^{j\omega}) = k \frac{\prod_{i=1}^{i=N_{zeros}} (j\omega - z_i)}{\prod_{i=1}^{i=N_{poles}} (j\omega - p_i)}. \quad (1)$$

A *pole-zero model* commonly consists of a gain value and the locations of poles and zeros for a specific sensor's frequency response. The poles are usually represented in radians as $-2\pi f_{hz}$, where f_{hz} is the pole frequency in Hz. In order to compute the response corrected auto and cross spectra, the units of the gain k must be scaled to obtain final spectra with Pa^2/Hz units. The *least significant bit* (lsb) of a digital system is the smallest step that can be represented by the digital output word of the ADC, and is often referred to as a *count*. lsb is defined as the full-scale voltage input limit of the ADC divided by the bit resolution of the ADC. For digital data outputs, the gain k must have units of lsb/Pa. When the analog gain in V/Pa is provided for a sensor's response, it is divided by the corresponding digitizer's ADC resolution in V/lsb to obtain units of lsb/Pa.

The response corrected auto and cross spectra between two time series x and y are computed as

$$P'_{xx}(f) = \frac{P_{xx}(f)}{H_x^*(e^{j\omega/2\pi}) H_x(e^{j\omega/2\pi})} \quad (2)$$

and

$$P'_{xy}(f) = \frac{P_{xy}(f)}{H_x^*(e^{j\omega/2\pi}) H_y(e^{j\omega/2\pi})}, \quad (3)$$

respectively. H^* denotes the complex conjugate of the frequency response H, f is the frequency in Hz, $P_{xx}(f)$ is the raw auto spectra of time series x (the same principle can be applied to time series y), and $P_{xy}(f)$ is the raw cross spectra between both time series.

A. Digital sensitivity measurement test

This test uses sinusoid pressure waves at multiple discrete frequency values to measure the digital sensitivity of

an acoustic sensor relative to a reference sensor. Single octave center frequency tones are generated with the signal generator; input sinusoidal parameters are 1Vpp amplitude, 0 phase, and 0 offset. More than 100 cycles of each tone are recorded. An octave band pass filter is first applied to each tone data with corner frequencies at $G^{-1/2N}f_0$ and $G^{1/2N}f_0$, where $G=10^{0.3}$, $N=1$, and f_0 is the octave center (i.e., tone) frequency (Garcés, 2013). Digital data records are then sliced into segments of user-specified consecutive cycles. In this study, data segments were set to 20 cycles. A three-parameter sine-fit algorithm (Merchant and Hart, 2011) is performed on the data segments to compute the sinusoidal amplitude and root-mean-square (RMS) error. Selected results are those with the highest signal-to-noise ratios. The sine-fit amplitude results for the reference sensor are multiplied by the sensor's digital sensitivity at the frequency of interest to obtain pressure units. The test sensor digital sensitivity is then estimated by dividing the reference amplitude in pressure units by the digital test amplitude.

B. Sensor frequency response test

This test uses a broadband noise pressure signal to verify the amplitude and phase response of a test sensor across the frequencies of interest relative to a reference sensor. A noise signal is generated by the signal generator with inputs 5 Vpp amplitude, 0 phase, and 0 offset; the signal is then fed into the rotary subwoofer for sound projection. The data from all sensors is retrieved as binary digital outputs and the response corrected auto and cross power spectra are computed. Raw spectra are first computed in lsb^2/Hz, and then corrected by the digital complex responses in lsb/Pa to obtain spectral units of Pa^2/Hz. All raw spectra are computed using Welch's method (Welch, 1967). The digital time series are first divided into 75% overlapping segments of the same size; the length of the segments is determined by the sample rate and desired spectral resolution. Each data segment is mean-subtracted and tapered with a *Hann* window of equal duration. The power spectrum is then computed by taking the square of the Fourier transform of the tapered and mean-subtracted data segments. To correct the spectral density for the windowing operation, each result is multiplied by a scaling factor $1/(fs\cdot\sum_{i=1}^{N}w^2)$, where fs is the sample rate and w is the windowing function of length N. The final power spectrum estimate is obtained by averaging the power spectra over the number of sections. All computed spectra are one-sided, where the power is attributed to positive frequencies only. Last, 95% confidence intervals (Bendat and Piersol, 1986a) of the power spectra are computed as $[n\hat{G}_{xx}(f)/\chi^2_{n;0.025}]\le G_{xx}(f)\le[n\hat{G}_{xx}(f)/\chi^2_{n;0.975}]$, where n is twice the number of spectral averages, $G_{xx}(f)$ is the spectral density at a given frequency f and $\hat{G}_{xx}(f)$ its estimate, and χ^2_ν the chi-square distribution with ν degrees of freedom.

The last step is to compute the response corrected relative amplitude $M(f)$, relative phase φ, and coherence C_{xy} on each pair of sensors as

$$M(f)=10\log_{10}\left(\frac{P'_{xx}(f)}{P'_{yy}(f)}\right), \tag{4}$$

$$\varphi=\arctan\left(\frac{Im(P'_{xy})}{Re(P'_{xy})}\right), \tag{5}$$

and

$$C_{xy}(f)=\frac{|P'_{xy}(f)|^2}{P'_{xx}(f)P'_{yy}(f)}. \tag{6}$$

The normalized random error (Bendat and Piersol, 1986b) of the coherence results is computed as $\sqrt{2}[1-C^2_{xy}(f)]/[|C_{xy}(f)|\sqrt{n_d}]$, where n_d is the number of spectral averages.

Given that the relative phase and coherence are functions of the cross spectrum, proper time alignment between the sensors must exist for the results from Eqs. (5) and (6) to be accurate. Lack of time alignment, however, does not affect the auto spectrum of the individual sensors, and a reliable value of relative magnitude can still be computed if the coherence is high.

Spectral averaging over 1/3-octave bands (Garcés, 2013) is performed on coherence and relative response data in order to smooth random variations in the narrowband spectrum. The 1/3-octave bands are computed with corner frequencies at $G^{-1/2N}f_0$ and $G^{1/2N}f_0$, where $G=10^{0.3}$, $N=3$, and f_0 is the octave center. A relative amplitude of 0 dB across the common passband of the test and reference sensors indicates identical spectral amplitudes. Similarly, a relative phase of 0 deg indicates identical spectral phase between the sensors. If the pole-zero model of the reference and test sensors perfectly represent their respective responses, then the relative amplitude and phase should be perfectly flat at 0 dB and 0 deg, respectively (Merchant and McDowell, 2014).

C. Sensor self-noise test

This test measures the self-noise of a sensor in a non-isolated environment. The sensor is left to record data overnight with all its ports sealed. Response corrected power spectral density levels are then computed as described in Sec. II B.

III. CHARACTERIZATION OF THE MB3 DIGITAL MICROBAROMETER RESPONSE ACROSS 0.01–4 Hz

The performance evaluation of the test sensor MB3d was assessed using a MB2000 as a reference. The MB2000 has a nominal analog sensitivity of 100 mV/Pa at 1 Hz, and was connected to 24-bit digitizer RefTek model 130-01 with nominal manufacturer ADC resolution 1.589 μV/lsb. The MB3d is reported to have a nominal analog sensitivity of 20 mV/Pa at 1 Hz and a nominal ADC resolution of 2.356 μV/lsb. When both test and reference sensors digitize their analog signals through 24-bit systems, the nominal digital sensitivity of the MB3d is 7.4 times greater than the nominal digital sensitivity of the MB2000/Reftek system. Sample rates were set to 100 Hz and digitizer gain values were set to unity.

TABLE I. Sine fit results with RMS error for MB3d digital sensitivity measurements. The algorithm's signal-to-noise values were 28, 29, and 39 dB at 1, 2, and 4 Hz octave center frequencies, respectively.

Frequency [Hz]	MB2000 pressure amplitude [Pa]	MB3d digital amplitude [lsb]	MB3d digital sensitivity [Pa/lsb]
1	3.430 ± 0.100	(3.085 ± 0.100)e+04	(1.112 ± 0.050)e-04
2	7.388 ± 0.200	(6.611 ± 0.200)e+04	(1.117 ± 0.050)e-04
4	3.759 ± 0.030	(3.320 ± 0.030)e+04	(1.132 ± 0.010)e-04

A. Digital sensitivity measurement

We obtained digital sensitivity values in Pa/lsb at 1, 2, and 4 Hz octave center frequencies for the MB3d test sensor relative to the MB2000. For this test, both sensors were placed with their ports capped on a padded surface to reduce vibration and connected to a manifold, which had one port open. The nominal digital sensitivity in Pa/lsb for the MB2000 was obtained by dividing the Reftek ADC resolution by the sensor's analog sensitivity. From the sine-fit results, we obtained digital sensitivities for the MB3d relative to the MB2000.

The digital sensitivity of the MB3d at 1 Hz was observed to be (1.112 ± 0.050)e-04 Pa/lsb, which deviates from its nominal 1.178 e-04 Pa/lsb value by 5.6% (0.48 dB). Merchant and McDowell (2014) found the analog sensitivities at 1 Hz of two MB3a sensors to deviate from the nominal value by 6.0% (0.51 dB) and 1.5% (0.13 dB), respectively, when tested in an isolation chamber. The observed values at 2 and 4 Hz shown in Table I differed from the measured value at 1 Hz by 0.52% (0.05 dB) and 1.85% (0.16 dB), respectively. Across the 1–4 Hz octave passbands, the observed digital sensitivities of the MB3d were flat (within 3 dB), with an average value of (1.120 ± 0.070)e-04 Pa/lsb (4.88% or 0.41 dB from nominal).

B. Sensor frequency response

We developed a pole-zero response model, described in Table II, for the MB3d test sensor based on the CEA reported bandwidth and the measured digital sensitivity at 1 Hz. We subsequently verified the MB3d frequency response (shown in Fig. 1) relative to the MB2000 using the same sensor configuration as in Sec. III A. In order to compare the digital outputs of the test and reference sensors, we scaled the nominal analog response model gain values in V/Pa provided by CEA to obtain digital gain units in lsb/Pa.

For this test we generated a 30-min acoustic noise signal and computed resulting Welch spectra with a fast Fourier transform window size of 16 384 samples (∼164 s). This allowed for a spectral resolution of 0.01 Hz, with approximately 44 averages across the record. The sensor configuration was left as described in Sec. III A.

The noise power spectral density levels in Fig. 2 and coherence analysis shown in Fig. 3 indicate coherence above 0.99 between the MB3d test sensor and MB2000 reference sensor across 0.01–4 Hz, with normalized random error (5.4 ± 4.0)e-06. The high coherence among the sensors serves to validate the relative response results within the passband of interest.

The relative amplitude 1/3-octave average results between the MB3 and MB2000 in Fig. 4(a) are flat to within 0.14 dB (1.6%) from 0.01 Hz up to the 4.0 Hz 1/3-octave band, with an observed 0.06 dB (0.75%) bias at 1 Hz. Relative phase results, shown in Fig. 4(b), show an average of 1.3 ± 1.8 deg across the same pass band, with a value of 1.8 deg at 1 Hz. The phase continues to rise above 1 Hz at a rate that suggests a time delay between the sensors of 5 ms, which is likely due to different digitizing systems. Merchant and McDowell (2014) measured the relative response of two MB3a sensors against a MB2000 sensor in an isolated chamber when connected to a common digitizer and found the relative magnitudes to be flat to within 0.3 dB (3.5%) and 1.15 dB (14.2%), respectively, across the 0.02–4 Hz IMS passband. The relative phase results found in the same study were seen to be flat to within 0.35 and 0.55 deg, respectively.

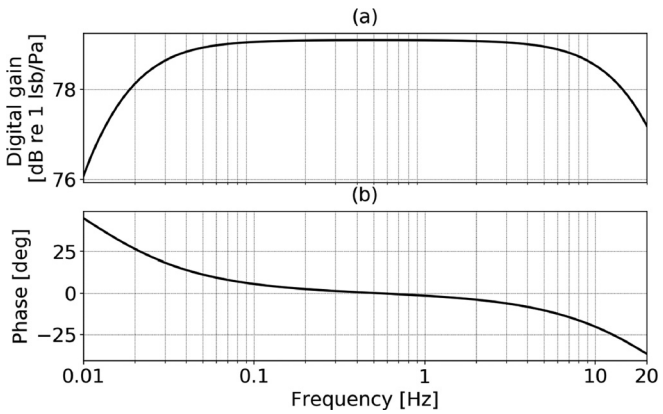

FIG. 1. Frequency response of the MB3d sensor based on pole-zero model presented in Table II. (a) Amplitude response in dB re 1 lsb/Pa. (b) Phase response in degrees.

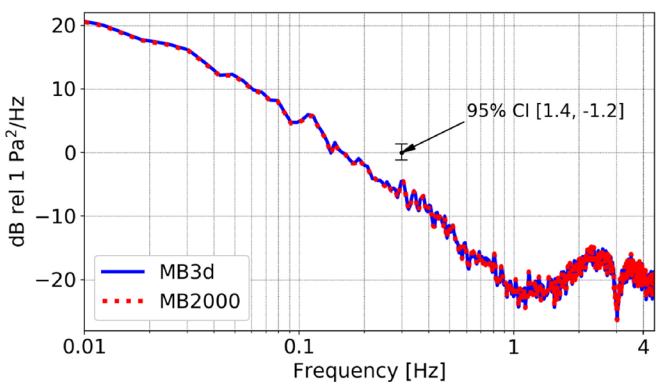

FIG. 2. (Color online) Noise power spectral density levels with 95% confidence interval (CI) [1.4, −1.2] dB re 1 Pa^2/Hz for MB3d and MB2000 across 0.01–4 Hz.

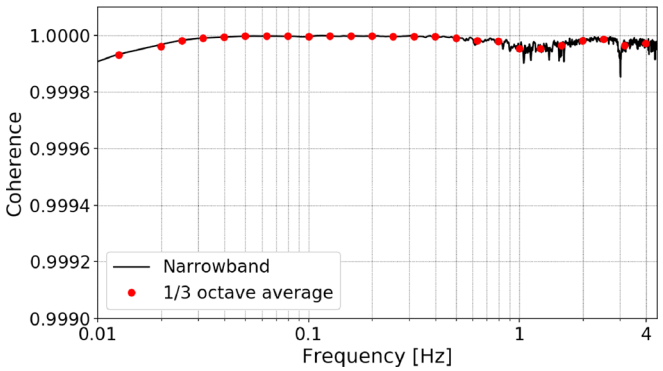

FIG. 3. (Color online) Noise coherence results for MB3d and MB2000 across 0.01–4 Hz. The solid line represents the coherence between the sensors. The filled circles represent 1/3-octave band averaging.

The results show that the MB3d corrected digital response is consistent with its parametric response model in a non-isolated environment across 0.01–4 Hz. Relative response results satisfy the sensitivity and phase specifications for sensors used in the CTBTO (2001) network (± 0.45 dB and $\pm 5°$, respectively, across the 0.02–4 Hz IMS pass band (Larsonner *et al.*, 2014).

C. Sensor self-noise

We measured and compared the self-noise of the sensors in a non-isolated environment. For this test, the sensors were disconnected from the manifold and left to record data overnight with their inlets sealed, using custom fittings for the MB3d.

Figure 5 shows isolated self-noise levels between the MB3d and MB2000 sensors. Coherence analysis results from Fig. 6 show lack of coherence between the sensors across 0.1–6 Hz; this incoherence satisfies the requirement described by Kromer *et al.* (2007), in which there should be no coherent signal present among the sensors for proper self-noise measurements. Figure 5 shows the MB3d has a lower self-noise relative to the MB2000 above 0.2 Hz. The CEA self-noise model for the MB3d is more than 10 dB below the LNM in an isolation chamber; the results agree with the CEA self-noise model from 0.15 to 4.0 Hz when averaged over 1/3-octave bands. The absence of microbarom infrasonic wave spectral curves across the 0.1–0.5 Hz passband (Christie and Campus, 2010) in Fig. 5 suggests proper sealing of the inlets. The self-noise levels for the MB3d in Fig. 5 are more than 10 dB above its CEA model across the 0.01–0.15 passband; coherence analysis in Fig. 6 also shows a slight coherence increase below 0.07 Hz. We suspect this discrepancy from the CEA noise-model across the 0.01–0.15 Hz passband is due to low-frequency atmospheric

TABLE II. Pole-zero response model for the MB3d sensor. The pole and zero locations were kept nominal. The digital gain value in lsb/Pa was corrected based on the measured digital sensitivity at 1 Hz shown in Table I.

Gain [lsb/Pa]	Zeros [rad]	Poles [rad]
1.527 e+06	$0+0j$	$-2\pi(0.01+0j)$ $-2\pi(27.0+0j)$

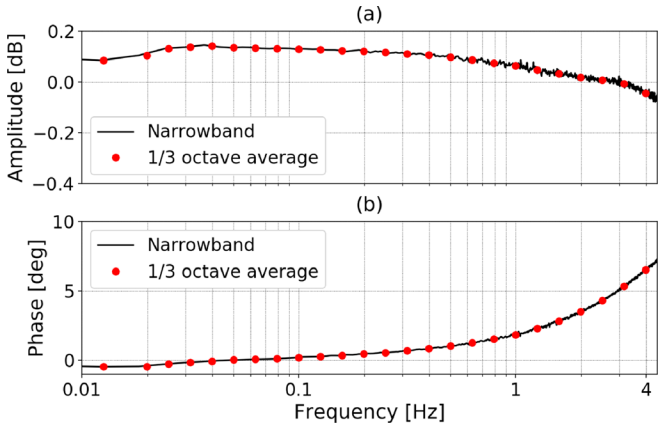

FIG. 4. (Color online) Noise response results for MB3d relative to MB2000 within the 0.01–4 Hz. (a) Relative amplitude between the sensors, computed as the ratio of their response corrected spectra. (b) Relative phase, computed as the angle of the response corrected cross-spectrum. Raw computations are represented by a solid line, while 1/3-octave band averaging is represented by the filled circles.

background signals feeding into the sensors in a non-isolated environment; these signals are usually attenuated inside isolation chambers.

Two unique spikes at 1 and 2 Hz can be discerned in the MB3d self-noise levels shown in Fig. 5. The sensor's embedded GPS is known to sample at 1 PPS. The 1 Hz spike is likely due to GPS sampling, while the 2 Hz spike corresponds to the first overtone. Both spikes are below the sensor's noise model levels. The MB3d self-noise across the 1.0 Hz 1/3-octave pass band (i.e., −84.92 dB) exceeds the IMS requirement of at least 18 dB below LNM at 1 Hz. Increased self-noise levels are seen for the MB3d sensor above 4 Hz when averaged over 1/3-octave bands, with a sharp increase on both sensors at 6 Hz. Coherence analysis results in Fig. 6 also show an abrupt increase in coherence between the sensors at 6 Hz. This suggests the presence of an external acoustic or seismic signal feeding into the sensors. Merchant and McDowell (2014) found the seismic sensitivity of the MB3a sensor to be visible in power spectra at frequencies above 4 Hz. The MB3a and MB3d sensors share

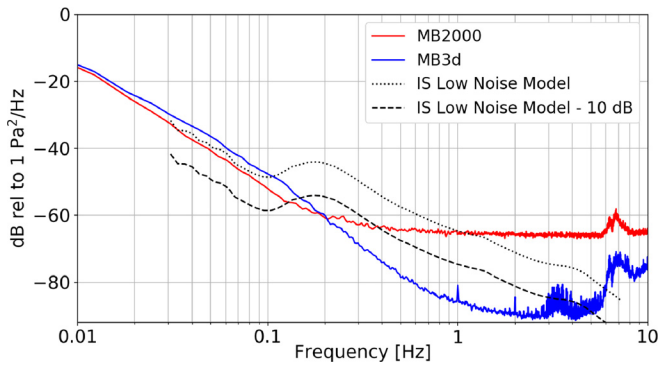

FIG. 5. (Color online) Response corrected self-noise power spectral density levels across the 0.01–10 Hz pass band for the MB2000 and MB3d, compared to the infrasound station (IS) low noise model (LNM) established by Bowman *et al.* (2007). The CEA self-noise model for the MB3d sensor is more than 10 dB below the IS LNM. Data were acquired from 2 a.m. to 5 a.m. local time; this time period is known for low wind and cultural noise.

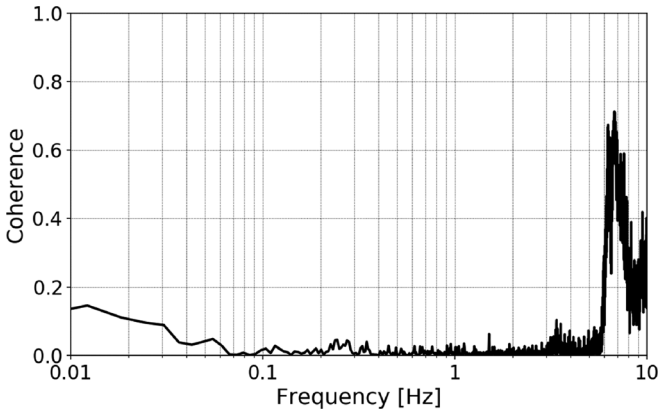

FIG. 6. Self-noise coherence results between the MB3d and MB2000 across the 0.01–10 Hz pass band. Data were acquired from 2 a.m. to 5 a.m. local time; this time period is known for low wind and cultural noise.

the same magnet and coil velocity transducer, which is more sensitive to seismic vibrations when compared to the LVDT of the MB2000. We hypothesize the high self-noise levels of the MB3d above 4 Hz are due to seismic vibrations. The results show that the MB3d is consistent with its manufacturer noise model in a non-isolated environment from 0.15 to 4 Hz; low-frequency atmospheric background signals and seismic sensitivity are self-noise increasing agents in the field.

IV. EVALUATION OF THE ANALOG BRÜEL & KJAER MICROPHONE TYPE 4193 MICROPHONE RESPONSE ABOVE 0.25 Hz

We obtained a digital sensitivity value and measured the response of the Brüel & Kjaer (B&K) microphone type 4193 test sensor against the MB3d, which was considered in Sec. III. The B&K sensor consists of an externally polarized analog microphone specially designed for infrasound, sonic boom, and pressure field measurements. The test sensor B&K microphone type 4193 was configured with infrasound adaptor UC-0211. We attached it to B&K preamplifier type ZC-0032, which was inserted to B&K hand held analyzer type 2250. Digitization of the B&K microphone data took place in the 24-bit digital interface embedded in the B&K hand held analyzer type 2250. We connected the MB3d and B&K sensors to a manifold and disconnected the B&K from power. All remaining ports on the MB3d were sealed, and one port was left open on the manifold. The MB3d sample rate was set to 20 Hz and unity digitizer gain. The B&K recorded at its lowest sample rate of 8000 Hz. In order to correct for the time between the test and reference sensors, we performed time correlation analysis on 30-s window containing the noise signal described in Sec. IV B. The MB3d data were upsampled to 8000 Hz in this particular process to obtain better time resolution. We preprocessed B&K data in this section by shifting the waveform by the delay found in the time correction algorithm, then downsampling the record to 20 Hz (with a decimation factor of 400) to match the MB3d sample rate, and reversing the polarity to match MB3d sensor polarity.

A. Digital sensitivity measurement

We obtained the digital sensitivities in Pa/lsb at 1, 2, and 4 Hz for the B&K test sensor relative to the MB3d values shown in Table I. We found in Sec. III C that the seismic sensitivity of the MB3d and MB2000 sensors increases above 4 Hz, which would make sinusoidal measurements with these sensors at 8 and 16 Hz unreliable.

The digital sensitivity of the B&K at 1 Hz was observed to be (9.002 ± 0.100)e-04 Pa/lsb, with deviations of 0.09% (0.01 dB) and 0.58% (0.05 dB) at 2 and 4 Hz, respectively (see Table III). Across the 1–4 Hz octave passband, the observed digital sensitivities of the B&K were flat (within 3 dB). These results suggest that the B&K response is consistent with its manufacturer response model, which specifies a flat response from below 1 Hz up to 20 000 Hz.

B. Sensor frequency response

We developed a pole-zero response model, described in Table IV, for the B&K sensor and verified it against the reference MB3d sensor. The B&K 4193 test microphone calibration sheet specifies a flat response beyond 4000 Hz, with a 3 dB low-end at 0.029 Hz. However, when connected to the preamplifier and hand held analyzer, the low corner frequency of the sensing system is between 0.1 and 1 Hz. We generated a response for the test sensor consistent with the measured digital sensitivity from Table III and the observed roll-off at the low corner frequency end. The response is shown in Fig. 7. Sensor configuration was kept as described in Sec. IV A.

For this test, we generated a 10-min noise acoustic signal and computed resulting Welch spectra with a fast Fourier transform window size of 4096 samples (∼205 s). This allowed for a spectral resolution of ∼0.01 Hz, with approximately 12 averages across the record. The low spectral resolution permits a coherence analysis with higher accuracy across the frequency bands at the expense of increasing the 95% confidence interval.

The noise power spectral density levels in Fig. 8 and coherence results in Fig. 9 indicate a coherence above 0.99 between the MB3d and B&K sensors from below 0.2 to beyond 7 Hz (above the upper limit of the MB3d evaluated passband and near where the anti-aliasing filter begins to operate). The normalized random error for the coherence across the passband is (2.4 ± 8.5)e-05. A downward spike in coherence is visible at 1 Hz. This is likely due to the GPS sampling of the MB3d sensor at 1 PPS (see Sec. III C). The

TABLE III. Sine fit results with RMS error for B&K digital sensitivity measurements. The algorithm's signal-to-noise values were 38, 38, and 40 dB at 1, 2, and 4 Hz octave center frequencies, respectively.

Frequency [Hz]	MB3d pressure amplitude [Pa]	B&K digital amplitude [lsb]	B&K digital sensitivity [Pa/lsb]
1	10.72 ± 0.10	(1.191 ± 0.010)e+04	(9.002 ± 0.100)e-04
2	7.029 ± 0.100	(7.801 ± 0.070)e+03	(9.010 ± 0.200)e-04
4	5.020 ± 0.040	(5.545 ± 0.040)e+03	(9.054 ± 0.100)e-04

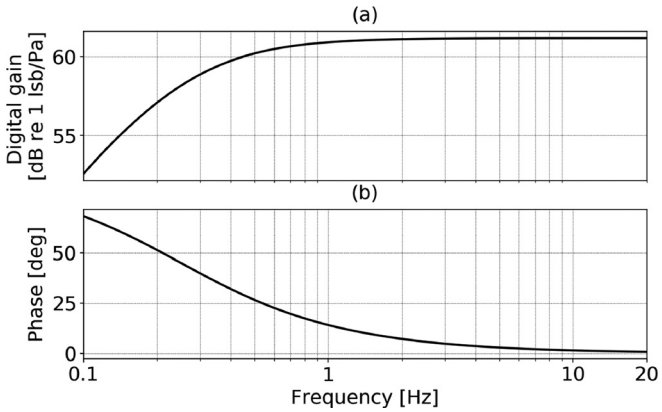

FIG. 7. Frequency response of the B&K sensor based on pole-zero model presented in Table IV. (a) Amplitude response in dB re 1 lsb/Pa. (b) Phase response in degrees.

high coherence among the sensors serves to validate the relative response results above the 0.2 Hz 1/3-octave band.

The relative amplitude 1/3-octave average results between the B&K test sensor and the MB3d in Fig. 10(a) are flat to within 0.40 dB (4.7%) across the 0.25–4.0 Hz 1/3-octave bands (upper limit of the MB3d evaluated passband). Relative phase results in Fig. 10(b) are −14.6 deg at 1 Hz. Across the 0.25–4.0 Hz passband, the relative phase has an average value of -22.8 ± 8.9 deg. Phase results are highly sensitive to time shifts and resampling. Given that the B&K is not a GPS synchronized system and that its lowest sample rate is 400 times greater than the sample rate of the MB3d, limitations arise in generating proper phase results between the B&K and MB3d. These results suggest that the amplitude response of the B&K sensor is flat above the 0.25 Hz 1/3-octave band, and can be used as a reference in digital calibrations.

V. EVALUATION OF THE IPRECISION SMARTPHONE MICROPHONE RESPONSE ACROSS 1–20 Hz

The test sensor consisted of iPrecision (iMic) smartphone microphone, which had been manufacturer-modified to decrease the lower frequency corner of the response. We obtained a digital sensitivity value in Pa/lsb for the test sensor and evaluated its response across the passband of interest

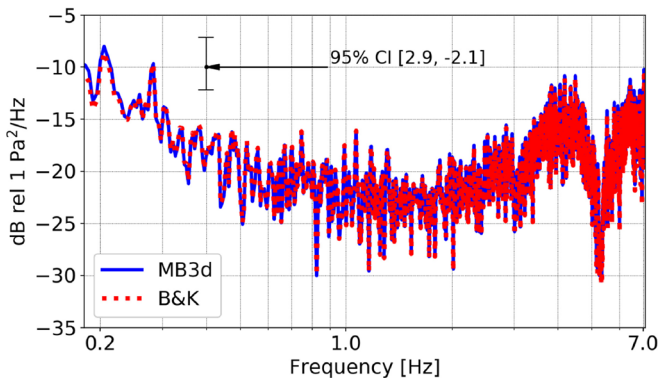

FIG. 8. (Color online) Noise power spectral density levels with 95% confidence interval (CI) [2.9, −2.1] dB re 1 Pa^2/Hz for B&K and MB3d across 0.18–7.1 Hz.

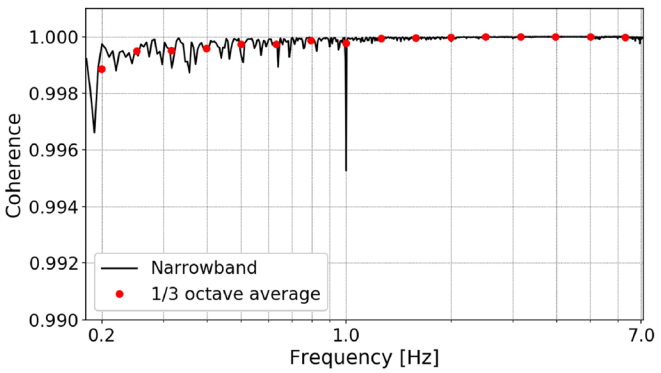

FIG. 9. (Color online) Noise coherence results for B&K and MB3d across 0.18–7.1 Hz. The solid line represents the coherence between the sensors. The filled circles represent 1/3-octave band averaging.

(1–20 Hz 1/3-octave bands). The reference was the Brüel & Kjaer Microphone type 4193 (B&K) sensor considered in Sec. IV. We disconnected both sensors from power and placed them inside a box with approximate dimensions $46 \times 33 \times 19\,cm^3$; the box was connected to a manifold, which had one port open. The iMic test sensor was connected to an iPhone 6 s running the *RedVox Infrasound app* for iOS; the *app* was set to record at 80 Hz sample rate. The B&K reference sensor recorded at a sample rate of 8000 Hz. In order to correct for the time between the test and reference sensors, we performed time correlation analysis on 30-s window containing the noise signal described in Sec. V B. The iMic data were upsampled to 8000 Hz in this particular process to obtain better time resolution. We preprocessed B&K data in this section by shifting the waveform by the delay found in the time correction algorithm, then downsampling the record to 80 Hz (with a decimation factor of 100) to match the iMic sample rate, and reversing the polarity to match iMic sensor polarity.

A. Digital sensitivity measurement

We obtained digital sensitivities in Pa/lsb at 8 and 16 Hz octave center frequencies for the iMic test sensor

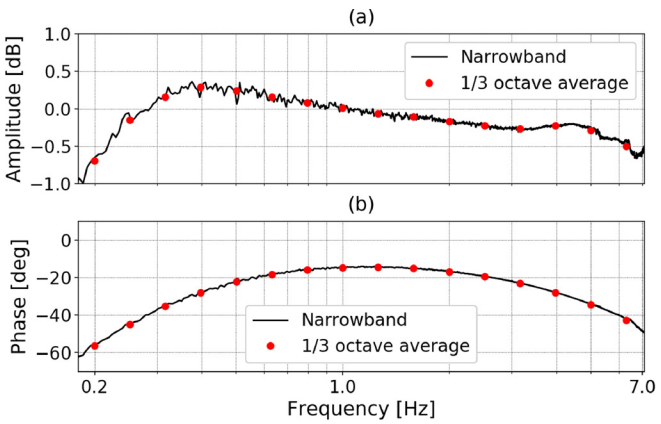

FIG. 10. (Color online) Noise response results for B&K relative to MB3d across 0.18–7.1 Hz. (a) Relative amplitude between the sensors, computed as the ratio of their response corrected spectra. (b) Relative phase, computed as the angle of the response corrected cross-spectrum. Raw computations are represented by a solid line, while 1/3-octave band averaging is represented by the filled circles.

TABLE IV. B&K pole-zero response model based on the digital sensitivity at 1 Hz presented in Table III and the observed low corner frequency roll-off at 0.25 Hz.

Gain [lsb/Pa]	Zeros [rad]	Poles [rad]
1.145 e+03	0 + 0j	$-2\pi(0.25 + 0j)$

relative to the B&K reference sensor. The iMic is reported to have a low corner frequency below 3 Hz, which would make octave sinusoid signal measurements at 1, 2, and 4 Hz unreliable. A single digital sensitivity value at 16 Hz was chosen for the test sensor; this was the sinusoidal record with the highest signal-to-noise (i.e., 35 dB) and coherence results.

B. Sensor frequency response

We developed a pole-zero response model, described in Table VI, for the iMic sensor and verified its response against the reference B&K sensor. The iMic test sensor is reported to have a flat amplitude response up to 20 000 Hz, with a 3 dB roll-off below 3 Hz. We generated a response for the test sensor based on the observed 3 dB roll-off frequencies and the measured digital sensitivity at 16 Hz. The iMic frequency response is shown in Fig. 11. We placed poles at the observed low corner frequencies (each pole was paired to a zero at origin) and corrected the digital gain to obtain the measured digital sensitivity at 16 Hz presented in Table V.

For this test we generated a 5-min acoustic noise signal and computed resulting spectra with a fast Fourier transform window size of 4096 samples (∼51.2 s). Spectral resolution was kept at ∼0.02 Hz while performing approximately 24 averages across the record. This allowed for sufficient smoothing of the random spectral variations while reducing errors in phase unwrapping at lower frequencies.

The noise power spectral density levels in Fig. 12 and coherence results in Fig. 13 indicate a coherence above 0.99 between the iMic test sensor and the B&K reference sensor across 0.97–22.4 Hz, with a normalized random error of (4.0 ± 3.4)e-04 across the passband. Relative amplitude 1/3-octave average results shown in Fig. 14(a) are flat to within 0.22 dB (2.6%) from the 1 Hz 1/3-octave pass band to beyond 20 Hz. Across the same passband, the relative phase of the sensors in Fig. 14(b) has an average value of −2.9 ± 4.2 deg. Though the relative phase is within 10 deg across the passband, time shifts and downsampling factors are limitations in a proper phase fitting of the sensors. The iMic sensor's amplitude response is consistent with its parametric response model in a non-isolated environment across 1–20 Hz.

VI. CONCLUSIONS

We have developed and characterized parametric response models for two next-generation digital acoustic sensors; we verified these responses against traceable, well-established analog sensors connected to external digitizers across the infrasound (i.e., 0.01–20 Hz) range in a non-isolated environment. We first evaluated the MB3 digital (MB3d) infrasound sensor against its MB2000 analog sensor predecessor, which was connected to a conventional external Reftek digitizer well known for its use in field experiments. We found the MB3d digital sensitivity at 1 Hz to be 5.6% from its nominal relative to the MB2000 nominal, and developed a pole-zero response model based on the measured digital sensitivity and the manufacturer-reported corner frequencies. Broadband measurements of a noise source indicated that the MB3d is consistent with its estimated response model across 0.01–4 Hz and meets the International Monitoring System requirements in a non-isolated environment. Self-noise measurements acquired over a 3-h period showed that the MB3d is consistent with its CEA self-noise model from 0.15 to 4 Hz in a non-isolated environment. We postulate that increased self-noise levels below 0.15 Hz are due to atmospheric background noise feeding into the sensor in a non-isolated environment, while higher levels above 4 Hz are due to seismic vibrations. This suggests that the performance of the MB3d, as per its manufacturer specifications, could be affected by external factors at frequencies outside the 0.15–4 Hz pass band in non-isolated environments.

We proceeded to develop a response model for an analog Brüel & Kjaer (B&K) Microphone type 4193 and evaluated it against the calibrated MB3d. We obtained the digital sensitivities at 1, 2, and 4 Hz for the B&K relative to the MB3d (shown in Table III). The results showed that the B&K frequency response is coherent with the MB3d and flat down to 0.40 dB (4.7%) across the sensors' common

TABLE V. Sine fit results with RMS error at 16 Hz for iMic digital sensitivity measurement. The algorithm's signal-to-noise value was 35 dB.

Frequency [Hz]	B&K pressure amplitude [Pa]	iMic digital amplitude [lsb]	iMic digital sensitivity [Pa/lsb]
16	(7.954 ± 0.100)e-01	(2.863 ± 0.030)e +06	(2.778 ± 0.050)e-07

TABLE VI. iMic (SN CQ10003) pole-zero response model based on the digital sensitivity presented in Table V and the observed 3 dB roll-off frequencies at 0.8, 1.5. and 3.5 Hz.

Gain [lsb/Pa]	Zeros [rad]	Poles [rad]
3.710 e+06	0 + 0j	$-2\pi(0.8 + 0j)$
	0 + 0j	$-2\pi(1.5 + 0j)$
	0 + 0j	$-2\pi(3.5 + 0j)$

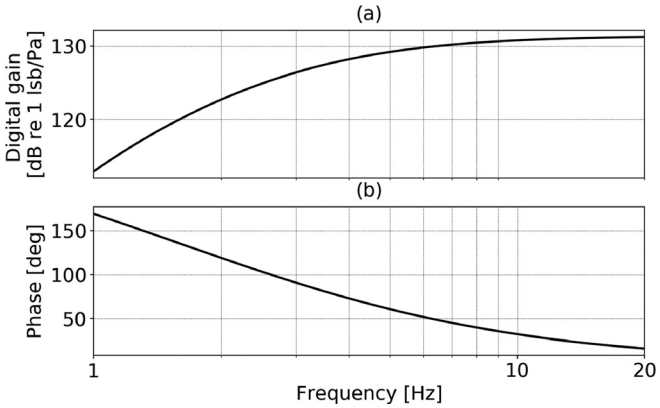

FIG. 11. Frequency response of the iMic sensor based on pole-zero model presented in Table VI. (a) Amplitude response in dB re 1 lsb/Pa. (b) Phase response in degrees.

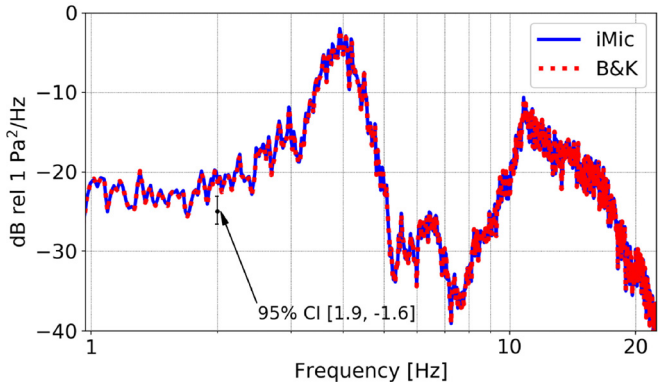

FIG. 12. (Color online) Noise power spectral density levels with 95% confidence interval (CI) [1.9, −1.6] dB re 1 Pa^2/Hz for iMic and B&K across 0.97–22.4 Hz.

passband (0.25–4 Hz). We subsequently calibrated an iPrecision (iMic) digital microphone sensor connected to an iPhone 6s against the chosen B&K reference. Sinusoidal tone measurements provided a digital sensitivity value in Pa/lsb for the iMic sensor at 16 Hz, shown in Table V. We developed a response model for the iMic sensor based on the measured digital sensitivity and corner frequencies. Measurements from a broadband noise source showed that the iMic amplitude response is coherent with the B&K reference and flat to within 0.22 dB (2.6%) across 1–20 Hz.

Two factors limit our ability to perform a proper fit of the phase portion of the complex responses for the B&K and iMic sensors. First, the B&K and iMic sensors are not GPS synced data acquisition systems, and thus have an inherent absolute timing error. Second, the process of decimation of the B&K data removed a significant amount of original samples. Phase responses are highly sensitive to time shifts and resampling, both of which were present in the work described in this article.

Signal processing results (i.e., high coherence and signal-to-noise) demonstrate the application of a portable rotary subwoofer as a controllable infrasound source during calibration experiments. We showed that digital calibrations performed in a non-isolated calibration room can provide useful and reproducible results. By overlapping the responses of the MB3d microbarometer (i.e., 0.01–4 Hz) and the iPrecision

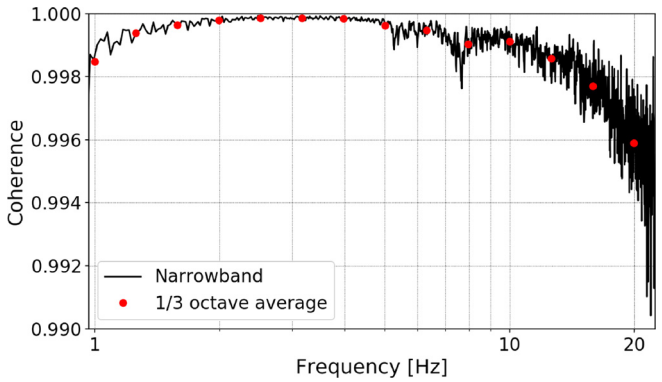

FIG. 13. (Color online) Noise coherence results for iMic and B&K across 0.97–22.4 Hz. The solid line represents the coherence between the sensors. The filled circles represent 1/3-octave band averaging.

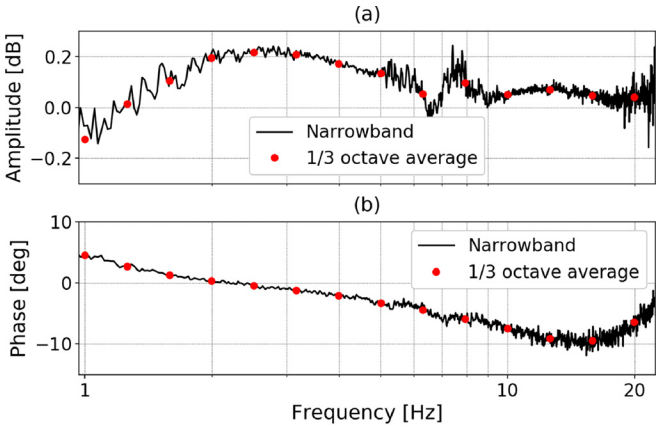

FIG. 14. (Color online) Noise response results for iMic relative to B&K across 0.97–22.4 Hz. (a) Relative amplitude between the sensors, computed as the ratio of their response corrected spectra. (b) Relative phase, computed as the angle of the response corrected cross-spectrum. Raw computations are represented by a solid line, while 1/3-octave band averaging is represented by the filled circles.

microphone (i.e., 1–20 Hz) we can potentially benchmark next-generation digital sensor performance across the 0.01–20 Hz (i.e., infrasound) pass band. Upon further validation of stability and repeatability, these parametric responses could be used as references in future pressure measurements and digital acoustic sensor calibrations.

ACKNOWLEDGMENTS

This work was supported by the Consortium for Verification Technology under Department of Energy National Nuclear Security Administration Award No. DE-NA0002534.

Audio Control (**2018**). Available at http://www.audiocontrol.com/pro-audio/mobile-solutions/iprecisionmic/ (Last viewed November 19, 2018).

Bendat, J. S., and Piersol, A. G. (**1986a**). "Statistical errors in basic estimates" in *Random Data Analysis Measurement Procedures*, 2nd ed. (Revised and Expanded) (John Wiley & Sons, Inc., New York), pp. 252–290.

Bendat, J. S., and Piersol, A. G. (**1986b**). "Statistical errors in advanced estimates" in *Random Data Analysis Measurement Procedures*, 2nd ed. (Revised and Expanded) (John Wiley & Sons, Inc., New York), pp. 291–324.

Bowman, J. R., Shields, G., and O'Brien, M. S. (**2007**). "Infrasound station ambient noise estimates and models," in *Infrasound Technology Workshop*, Tokyo, Japan, 13–16 November.

Brüel, D., and Kjaer, V. (**1995**). *Technical Documentation, Microphone Handbook* (available at https://www.bksv.com/media/doc/be1373.pdf), 216 pp.

CEA/DAM (**2009**). "MB2000 and MB2005 microbarometers," available at http://www-dase.cea.fr/public/dossiers_thematiques/microbarometres/description_en.html (Last viewed November 19, 2018).

Christie, D. R., and Campus, P. (**2010**). "The IMS infrasound network: Design and establishment of infrasound stations," in *Infrasound Monitoring for Atmospheric Studies*, edited by A. Le Pichon, E. Blanc, and A. Hauchecorne (Springer, New York), pp. 29–75.

CTBTO (**2001**). "The Global Verification Regime and the International Monitoring System," CTBTO Preparatory Commission, Vienna International Centre, Vienna, Austria.

Eminent Technologies (**2018**). Available at http://www.eminent-tech.com/ (Last viewed November 19, 2018).

Garcés, M. A. (**2013**). "On infrasound standards, Part 1: Time, frequency and energy scaling," InfraMatics **2**(2), 13–35.

Kromer, R. P., Hart, D. M., and Harris, J. M. (**2007**). "Test definitions for the evaluation of infrasound sensors," Sandia National Laboratories Technical Report No. SAND2007-5038.

Larsonner, F., Uszakiewicz, H-G., and Mende, M. (**2014**). "Infrasound sensors and their calibration at low frequency," in *INTERNOISE 2014 43rd International Congress on Noise Control Engineering: Improving the World Through Noise Control*, Melbourne, Australia, 16–19 November.

Marcillo, O., Johnson, J. B., and Hart, D. (**2012**). "Implementation, characterization, and evaluation of an inexpensive low-power low-noise infrasound sensor based on a micromachined differential pressure transducer and mechanical filter," J. Atmos. Oceanic Technol. **29**, 1275–1284.

Merchant, J., and Hart, D. (**2011**). "Component evaluation testing and analysis algorithms," Sandia National Laboratories Technical Report No. SAND2011-8265.

Merchant, J., and McDowell, K. (**2014**). "MB3a infrasound sensor evaluation," Sandia National Laboratories Technical Report No. SAND2014-20108.

Ollivier, S., Salze, E., Averiyanov, M., Yuldashev, P., Khokhlova, V., and Blanc-Benon, P. (**2012**). "Calibration method for high frequency microphones," in *Proceedings of the Acoustics Nantes Conference*, Nantes, France, April 2012.

Park, J., Garcés, M. A., and Thigpen, B. (**2009a**). "The rotary subwoofer: A controllable infrasound source," J. Acoust. Soc. Am. **125**(4), 2006–2012.

Park, J., and Robertson, J. (**2009b**). "A portable infrasound generator," J. Acoust. Soc. Am. **125**(4), EL148–EL151.

Redvox (**2014**). Infrasound Recorder for Apple iOS (Version 2.1.1) [Mobile application software], available at https://itunes.apple.com/ (Last viewed November 19, 2018).

Refraction Technology Inc. (**2011**). "130-01 Operations: Startup," available at http://nappe.wustl.edu/SPREE/instrument-other-documentation/from-RefTek/130_startup_01.pdf, 121 pp. (Last viewed November 19, 2018).

Seismowave (**2015**). "MB3d Infrasound Sensor," available at http://seismowave.com/medias/documents/MB3d2.pdf (Last viewed November 19, 2018).

Welch, P. D. (**1967**). "The use of the fast Fourier transform for the estimation of power spectra," IEEE Trans. Audio Electroacoust. **AU-15**(2), 70–73.